

This is a repository copy of *Rapid compensatory evolution can rescue low fitness symbioses following partner-switching*.

White Rose Research Online URL for this paper:

<https://eprints.whiterose.ac.uk/175451/>

Version: Accepted Version

---

**Article:**

Sørensen, Megan E S, Wood, A. Jamie orcid.org/0000-0002-6119-852X, Cameron, Duncan D. et al. (1 more author) (2021) Rapid compensatory evolution can rescue low fitness symbioses following partner-switching. *Current Biology*. pp. 1-13. ISSN 0960-9822

<https://doi.org/10.1016/j.cub.2021.06.034>

---

**Reuse**

This article is distributed under the terms of the Creative Commons Attribution-NonCommercial-NoDerivs (CC BY-NC-ND) licence. This licence only allows you to download this work and share it with others as long as you credit the authors, but you can't change the article in any way or use it commercially. More information and the full terms of the licence here: <https://creativecommons.org/licenses/>

**Takedown**

If you consider content in White Rose Research Online to be in breach of UK law, please notify us by emailing [eprints@whiterose.ac.uk](mailto:eprints@whiterose.ac.uk) including the URL of the record and the reason for the withdrawal request.

## **Rapid compensatory evolution can rescue low fitness symbioses following partner-switching**

Megan E S Sørensen<sup>1</sup>, A Jamie Wood<sup>2</sup>, Duncan D Cameron<sup>1</sup>, Michael A Brockhurst<sup>3\*</sup>

1. Department of Animal and Plant Sciences, University of Sheffield, Sheffield S10 2TN
2. Department of Biology, University of York, York YO10 5DD
3. Division of Evolution and Genomic Sciences, School of Biological Sciences, University of Manchester, Manchester M13 9PT

\*Lead contact Michael A. Brockhurst.

**Email:** [michael.brockhurst@manchester.ac.uk](mailto:michael.brockhurst@manchester.ac.uk)

**Twitter:** @BrockhurstLab

## 1 **Summary**

2 Partner-switching plays an important role in the evolution of symbiosis, enabling local  
3 adaptation and recovery from the breakdown of symbiosis. Because of intergenomic  
4 epistasis, partner-switched symbioses may possess novel combinations of phenotypes but  
5 may also exhibit low fitness due to their lack of recent coevolutionary history. Here, we  
6 examine the structure and mechanisms of intergenomic epistasis in the *Paramecium-*  
7 *Chlorella* symbiosis and test if compensatory evolution can rescue initially low fitness  
8 partner-switched symbioses. Using partner-switch experiments coupled with metabolomics  
9 we show evidence for intergenomic epistasis wherein low fitness is associated with elevated  
10 symbiont stress responses either in dark or high irradiance environments, potentially owing  
11 to mismatched light management traits between the host and symbiont genotypes.  
12 Experimental evolution under high light conditions revealed that an initially low fitness  
13 partner-switched non-native host-symbiont pairing rapidly adapted, gaining fitness  
14 equivalent to the native host symbiont pairing in less than 50 host generations.  
15 Compensatory evolution took two alternative routes: Either, hosts evolved higher symbiont  
16 loads to mitigate for their new algal symbiont's poor performance, or the algal symbionts  
17 themselves evolved higher investment in photosynthesis and photoprotective traits to better  
18 mitigate light stress. These findings suggest that partner-switching combined with rapid  
19 compensatory evolution can enable the recovery and local adaptation of symbioses in  
20 response to changing environments.

21

22 **Keywords:** Symbiosis, Experimental evolution, photosymbiosis, partner-switching

23

## 24 **Introduction**

25 Beneficial symbioses have an inherent potential for conflict between the symbiotic partners.  
26 This can drive the breakdown of symbiosis if environmental conditions change the net  
27 benefit of interacting or if the pursuit of individual fitness favours cheating <sup>1</sup>. Both situations  
28 can select for partner-switching to recombine symbiotic partnerships <sup>2</sup>. Partner-switching can

29 provide hosts with access to favourable symbiotic phenotypes to overcome maladaptation to  
30 the prevailing environmental context<sup>3</sup> or restore symbiont function following breakdown<sup>4,5</sup>.  
31 The generation of phenotypic plasticity through partner-switching arises from genetic  
32 variation of hosts ( $G^H$ ) and symbionts ( $G^S$ ) and intergenomic epistasis<sup>6</sup>, that is, genetic  
33 variation for the outcome of symbiosis in the form of host genotype by symbiont genotype  
34 interactions ( $G^H \times G^S$ ) for symbiotic traits or fitness. Furthermore, the fitness effects of  
35 symbiosis can be mediated by the environmental context<sup>7</sup>, causing host-genotype-by-  
36 symbiont-genotype-by-environment interactions ( $G^H \times G^S \times E$ ). A consequence of  $G^H \times G^S \times$   
37  $E$  interactions is that there is unlikely to be an optimal host-symbiont pairing across all  
38 environments, further driving selection for partner-switching or dynamic coevolution of the  
39 symbiosis<sup>8</sup>. As such, partner-switching can enable niche-expansion by hosts<sup>9,10</sup> and  
40 provide a mechanism by which hosts can adapt to local environmental conditions faster than  
41 through *de novo* adaptation of the current symbiont<sup>11,12</sup>.

42  
43 Newly interacting partner-switched host-symbiont pairings are, however, unlikely to be co-  
44 adapted due to their lack of recent coevolutionary history and may, therefore, initially have  
45 low fitness<sup>13-15</sup>. Indeed, despite the adaptive potential of partner-switching, new host-  
46 symbiont pairings, like genetic mutations, may more often be deleterious than beneficial to  
47 host fitness due to phenotypic mismatches or genetic incompatibilities. This has been  
48 observed in a range of symbiotic interactions: for example, a newly acquired *Symbiodinium*  
49 endosymbiont was found to translocate less fixed carbon than the native symbiont to its  
50 cnidarian host<sup>13</sup>; novel bacterial endosymbionts had reduced vertical transmission rates in  
51 aphid hosts<sup>14</sup>; and novel *Wolbachia* endosymbionts reduced the reproductive fitness of  
52 *Drosophila simulans*<sup>15</sup>. How then do newly-formed, poorly co-adapted host-symbiont  
53 pairings become stable, beneficial symbioses? We hypothesise that rapid compensatory  
54 evolution (that is adaptation of the host, the symbiont, or both to ameliorate the deleterious  
55 fitness effects of partner-switching) could allow partner-switched symbioses to overcome  
56 their initially low fitness. Indeed, there is some, albeit limited, experimental evidence to

57 support this idea: For example, the high fitness cost of newly acquired *Spiroplasma*  
58 endosymbionts in *Drosophila melanogaster* was ameliorated within only 17 host  
59 generations<sup>16</sup>, although the underlying mechanisms of this fitness recovery remain unknown.  
60 Furthermore, horizontal gene transfers were found to have caused the rapid evolution of  
61 nonsymbiotic strains of rhizobia bacterial symbionts into symbiotic partners in field-site tests  
62 with *Lotus* plant hosts<sup>17</sup>.

63

64 The microbial symbiosis between *Paramecium bursaria* and *Chlorella* provides an  
65 experimentally tractable model system to study intergenomic epistasis and the underlying  
66 molecular mechanisms. The ciliate host, *P. bursaria*, is a single-celled eukaryote, and each  
67 host cell contains 100-600 cells of the algal endosymbiont, *Chlorella*<sup>18,19</sup>. The *P. bursaria* -  
68 *Chlorella* symbiosis is based on a primary nutrient exchange of fixed carbon from the  
69 photosynthetic alga for organic nitrogen from the heterotrophic host<sup>18,20</sup>. *Chlorella* algal  
70 symbionts are primarily vertically transmitted to daughter cells at *Paramecium* cell division,  
71 although additional algal symbionts can also be acquired from the environment by  
72 ingestion<sup>21,22</sup>. This symbiosis is geographically widespread and genetically diverse, in part  
73 due to multiple independent acquisitions of algal symbionts by *P. bursaria*. The primary  
74 nutrient exchange is convergent among these origins<sup>23</sup>. This facilitates partner-switching, but  
75 concurrent divergence in other metabolic traits can cause phenotypic mismatches in partner-  
76 switched host-symbiont pairings<sup>23</sup>. Here, using experimental partner-switches, we examined  
77 the pattern and mechanisms of intergenomic epistasis for three diverse host-symbiont  
78 strains, observing significant  $G^H \times G^S \times E$  interactions for host-symbiont growth rate and  
79 symbiont load (that is the number of symbionts per host cell), together with corresponding  
80 differences in metabolism. We then experimentally evolved a low fitness partner-switched  
81 host-symbiont pairing for ~50 host generations. We observed rapid compensatory evolution  
82 by hosts and symbionts that improved fitness to equal to that of the native host-symbiont  
83 pairing mediated by evolved changes in host control of symbiont load and in symbiont  
84 metabolism.

85

## 86 **Results**

87 **Intergenomic epistasis for host-symbiont growth and symbiont load.** We constructed  
88 all possible host-symbiont genotype pairings ( $n = 9$ ) of 3 diverse strains of *Paramecium-*  
89 *Chlorella* and confirmed their identity by diagnostic PCR (Figure S1). We measured the  
90 growth reaction norm of each host-symbiont pairing across a light gradient (Figure 1a). All  
91 host-symbiont pairings showed the classic photosymbiotic reaction norm<sup>24</sup>, such that growth  
92 rate increased with irradiance, but we observed a significant  $G^H \times G^S \times E$  interaction for  
93 host-symbiont growth rate ( $G^H \times G^S \times E$  interaction, ANOVA,  $F_{17,162} = 18.81$ ,  $P < 0.001$ )  
94 consistent with intergenomic epistasis. This was driven by contrasting effects of symbiont  
95 genotype on growth in the different host backgrounds across light environments. In the HK1  
96 and HA1 host-backgrounds, similar growth reaction norms with light were observed for each  
97 symbiont genotype, whereas in the 186b host background the growth reaction norm varied  
98 according to symbiont genotype. Interestingly, the native 186b host-symbiont pairing had  
99 both the lowest intercept and the highest slope, indicating that in the 186b host background  
100 the native algal symbiont genotype was costlier in the dark (Welch t-test on native versus  
101 non-native symbionts  $t(7.29) = -10.13$ ,  $p = < 0.001$ ) yet more beneficial in high-light  
102 environments than non-native algal symbiont-genotypes (Welch t-test on native versus non-  
103 native symbionts  $t(10.44) = 3.21$ ,  $p = < 0.01$ ).

104

105 *P. bursaria* host cells regulate their algal symbiont load (i.e. the number of symbionts per  
106 host cell) according to light irradiance to maximise the benefit-to-cost ratio of symbiosis,  
107 such that, for naturally occurring host-symbiont pairings, symbiont load peaks at  
108 intermediate irradiance and is reduced both in the dark and at high irradiance<sup>24–26</sup>. To test if  
109 regulation of symbiont load varied among host-symbiont pairings, we measured symbiont  
110 load across the light gradient as the intensity of single-cell fluorescence, which is correlated  
111 with the number of symbionts per host cell<sup>19</sup>, by flow cytometry (Figure 1b). All host-  
112 symbiont pairings showed the expected unimodal symbiont load curve with light, but

113 nevertheless we observed a significant  $G^H \times G^S \times E$  interaction for symbiont load ( $G^H \times G^S \times$   
114  $E$  interaction, ANOVA,  $F_{17,162} = 3.78$ ,  $P < 0.001$ ) consistent with intergenomic epistasis.  
115 Whereas, in the HA1 host similar symbiont load reaction norms were observed for each  
116 symbiont genotype, for the HK1 and 186b host backgrounds the form of the symbiont load  
117 reaction norms varied according to symbiont genotype. In the HK1 host, the magnitude of  
118 the symbiont load varied by symbiont genotype, such that higher symbiont loads were  
119 observed for the native compared to the non-native symbiont-genotypes. In the 186b host,  
120 peak symbiont load occurred at different light levels according to symbiont genotype, such  
121 that for the native symbiont the symbiont load curve peaked at a higher light intensity when  
122 compared to the non-native symbionts. (For the full output of the polynomial model, see  
123 Data S1.) Because symbiont load is primarily host-controlled in this system<sup>24,25</sup>, this  
124 suggests that the HK1 and 186b host-genotypes discriminated among symbiont-genotypes,  
125 and then regulated symbiont load accordingly.

126

127 **Metabolic mechanisms of intergenomic epistasis.** To investigate the potential metabolic  
128 mechanisms underlying the observed intergenomic epistasis we performed untargeted  
129 global metabolomics with ESI-ToF-MS independently for the host and symbiont metabolite  
130 fractions for each host-symbiont pairing across the light gradient<sup>23</sup>. Light irradiance was the  
131 primary driver of differential metabolism for both host and symbiont, however, host-  
132 dependent differences in the metabolism of symbiont-genotypes could be detected. For the  
133 symbiont metabolite fraction subset by host-genotype, we observed native versus non-native  
134 clustering of symbiont metabolism only when associated with the 186b host-genotype  
135 (Figure S2). This is consistent with the larger phenotypic differences in growth and symbiont  
136 load observed among host-symbiont pairings with the 186b host-genotype compared to with  
137 either the HK1 or HA1 host-genotypes. We therefore focused our analyses on comparing the  
138 metabolic profiles of the different symbiont genotypes within the 186b host background.  
139 Pairwise contrasts of the symbiont-genotypes in the 186b host-genotype background  
140 revealed a range of candidate symbiont metabolites which distinguished the native pairing

141 from either non-native host-symbiont pairing. Putative identifications included, in the dark,  
142 elevated levels of candidate metabolites associated with stress responses (stress-  
143 associated hormones, jasmonic acid and abscisic acid, and stress associated-fatty acids,  
144 such as arachidonic acid) but reduced production of vitamins and co-factors by the native  
145 symbiont, compared to the non-native symbionts (Table S1). At high irradiance, the native  
146 symbiont showed higher levels of candidate metabolites in central metabolism, hydrocarbon  
147 metabolism and of biotin (vitamin B7), compared to the non-native symbionts (Table S1). In  
148 contrast, the non-native symbionts produced elevated levels, relative to native symbionts, of  
149 a candidate glutathione derivative; glutathione is an antioxidant involved in the ascorbate-  
150 glutathione cycle that combats high UV stress through radical oxygen scavenging <sup>27,28</sup>.  
151 Together, these data suggest that impaired host-symbiont performance was associated with  
152 elevated symbiont stress responses and that symbiont genotypes varied in their requirement  
153 for host photoprotection, providing a putative mechanism underlying intergenomic epistasis.

154

155 **Rapid compensatory evolution can rescue an initially low fitness partner-switched**  
156 **symbiosis.** The partner-switched pairing of the 186b host with the HK1 symbiont showed  
157 substantially reduced growth at high light relative to the native 186b host-symbiont pairing.  
158 To test if this fitness deficit could be overcome through compensatory evolution, we  
159 established six replicate populations of each of these two symbiotic partnerships (i.e., the  
160 186b host with the 186b algal symbiont and the 186b host with the HK1 algal symbiont),  
161 which were propagated by weekly serial transfer for 25 transfers (approximately 50 host  
162 generations) at a high light regime (50 $\mu$ E; 14:10 L:D). The growth rate per transfer was  
163 higher for the native pairing than the non-native pairing (Figure S3a) (linear mixed effect  
164 model, HK1 symbiont fixed effect of  $-0.08 \pm 0.006$ , T-value =  $-14.126$ , see Data S1 for full  
165 statistical output), but increased over time for both pairings (transfer number fixed effect  
166  $0.001 \pm 0.0004$ , T-value =  $3.088$ ). To test for adaptation, we compared the fitness effect of  
167 symbiosis at the beginning and the end of the transfer experiment by direct competition of  
168 either the ancestral or evolved host-symbiont pairings against the symbiont-free ancestral



169 186b host genotype across a light gradient. Fitness at the start of the evolution experiment  
170 of symbiotic relative to non-symbiotic hosts increased more steeply with irradiance for the  
171 native than the partner-switched non-native pairing (Figure 2), but this difference had  
172 disappeared by the end of the evolution experiment, such that both the native and non-  
173 native host-symbiont pairings showed increasing fitness relative to non-symbiotic hosts with  
174 increasing irradiance (symbiont genotype by light intensity by transfer number interaction  
175 term: ANOVA,  $F_{7,45} = 6.20$ ,  $P < 0.001$ ). Indeed, at  $50 \mu\text{E m}^{-2} \text{s}^{-1}$ , the light level used in the  
176 selection experiment, the large fitness deficit observed between the native and non-native  
177 pairing at the beginning of the experiment had been completely compensated. Comparison  
178 of the growth reaction norms of the evolving populations over time suggested that this  
179 amelioration occurred rapidly: By the tenth transfer, the native and non-native host-symbiont  
180 pairings showed equivalent growth responses to light (Welch t-test  $t(45.96) = -0.26$ ,  $p =$   
181  $0.80$ ), in contrast to their substantially different ancestral growth reaction norms observed at  
182 the start of the evolution experiment (Welch t-test  $t(35.79) = 3.59$ ,  $p = < 0.001$ ) (Figure S3b).  
183 These data suggest that newly established partner-switched symbioses can rapidly achieve  
184 equivalent growth performance and fitness benefits as the native host-symbiont pairing by  
185 compensatory evolution.

186

187 **Evolved changes in symbiont load regulation and metabolism.** To understand the  
188 mechanisms of compensatory evolution, we first compared the symbiont load reaction  
189 norms of the ancestral and evolved native and non-native pairings (Figure 3). Both ancestral  
190 host-symbiont pairings showed the expected unimodal symbiont load curve with light, albeit  
191 with higher symbiont loads for the native compared to the non-native pairing at the highest  
192 light level,  $50 \mu\text{E m}^{-2} \text{s}^{-1}$  irradiance, as used in the transfer experiment. By the end of the  
193 evolution experiment, the shape of the symbiont load reaction norms were altered in both  
194 the native and non-native pairings. Most notably, at  $50 \mu\text{E m}^{-2} \text{s}^{-1}$  irradiance, whereas the  
195 non-native pairing had increased symbiont load, symbiont load had decreased in the native  
196 pairing, such that symbiont load was now higher in the non-native pairing (transfer by

197 symbiont genotype interaction at high light: ANOVA,  $F_{3,20} = 16.88$ ,  $P < 0.001$ ). Higher  
198 symbiont loads may therefore have contributed to the observed increased fitness of evolved  
199 compared to ancestral non-native pairings in the high light environment.

200

201 Next, to investigate the potential underlying metabolic mechanisms, we performed  
202 untargeted metabolomics analyses on the separated *Chlorella* and *P. bursaria* fractions from  
203 samples taken the start and end of the evolution experiment grown at  $50 \mu\text{E m}^{-2} \text{s}^{-1}$ . The  
204 ancestral *P. bursaria* and *Chlorella* metabolic profiles of native and non-native host-symbiont  
205 pairings could be clearly distinguished (Figure 4). At the end of the evolution experiment, *P.*  
206 *bursaria* metabolism displayed a high degree of apparent convergence between hosts  
207 evolved with the native versus the non-native symbionts (Figure 4a,c). This was driven by  
208 decreased levels of compounds of central metabolism (such as pyruvate and TCA cycle  
209 intermediates, antioxidants, lipids, and some amino acids) (Table S2), suggesting either  
210 increased pathway completion or a reduced metabolic rate, both of which can lead to  
211 increased efficiency. In addition, we observed increased levels of the amino acid cysteine  
212 and a shikimate pathway component in hosts evolved with the native versus the non-native  
213 symbionts (Figure S4). Levels of algal-cell degradation components (Figure S4), such as  
214 cell-wall degradation product chitotriose, were increased in some replicates of hosts evolved  
215 with either symbiont, potentially suggesting increased digestion of *Chlorella*, which is a  
216 known mechanism by which hosts control their symbiont load<sup>29,30</sup>.

217

218 In contrast, evolved changes to the metabolic profiles of the algal symbiont genotypes  
219 showed less consistent differences among treatments (Figure 4b,d). Whereas all replicates  
220 of the native 186b *Chlorella* evolved in a similar direction, the replicates of the non-native  
221 HK1 *Chlorella* evolved in two different directions. Two of the HK1 replicates took a similar  
222 trajectory to the 186b symbionts, while the remaining four replicates all followed an  
223 alternative evolutionary trajectory. The group of four HK1 replicates that diverged during the  
224 experiment had lower production of metabolites within core aspects of metabolism, such as

225 lipids, amino acids and carbohydrates. The second group, including the remaining two HK1  
226 replicates and all the 186b replicates, had for the most part higher production of metabolites  
227 within primary metabolism pathways, particularly within lipids and carbohydrates, as well as  
228 a key chlorophyll compound, a photo-protective carotenoid (though not for all of the 186b  
229 replicates), and secondary metabolites with potential antioxidant properties (Figure S4,  
230 Table S2). This greater investment into photosynthesis and photo-protection may improve  
231 carbon transfer to the host <sup>31,32</sup>, and decrease light stress, which aligns with the decrease in  
232 host antioxidants. Interestingly, the two HK1 replicates that appeared to converge  
233 metabolically with the native symbionts had a lower increase in symbiont load compared to  
234 the replicates that metabolically diverged (Table S3). This implies that the evolution of  
235 metabolism and symbiont load were linked, and that overall two alternative strategies of  
236 compensatory evolution emerged: either to have fewer, more beneficial symbionts or to have  
237 more, less-beneficial symbionts.

238

## 239 **Discussion**

240 Partner switching plays an important role in the evolution of a wide range of symbioses  
241 <sup>2,4,5,33,34</sup> enabling adaptation to changing environments and recovery from the breakdown of  
242 symbiosis. Because of intergenomic epistasis, partner-switched host-symbiont pairings may  
243 possess novel adaptive phenotypes, but will sometimes exhibit low fitness associated with  
244 mismatches between host and symbiont traits, owing to their lack of recent coevolutionary  
245 history <sup>14,15,35</sup>. In the *Paramecium-Chlorella* symbiosis, low fitness host symbiont pairings  
246 were associated with elevated symbiont stress responses either in dark or high irradiance  
247 environments, suggesting that mismatching light management traits between host and  
248 symbiont genotypes may be a potential cause of intergenomic epistasis. This corresponds  
249 with findings from other photosynthetic symbioses, including coral-*Symbiodinium* and *Hydra*-  
250 *Chlorella*, where mismatching thermal and light stress tolerances contribute to the  
251 breakdown of symbiosis <sup>36-39</sup>. Low fitness, partner-switched host-symbiont pairings were  
252 rescued by compensatory evolution, which took one of two routes: Either, hosts evolved

253 higher symbiont loads to mitigate for their new algal symbiont's poor performance, or the  
254 algal symbionts themselves evolved higher investment in photosynthesis and  
255 photoprotection traits to better mitigate light stress. Given that symbiont load varies with light  
256 due to host control<sup>24,25</sup>, it seems likely that the evolved change in symbiont load is due to  
257 phenotypic plasticity through altered host regulation, whereas the evolved change in algal  
258 photosynthetic metabolism could be due to either genetic or physiological adaptation by the  
259 symbionts. Both strategies increased growth of the non-native host-symbiont pairing, leading  
260 to higher fitness equivalent to that of the native host-symbiont pairing. Together, these data  
261 suggest that, partner-switching combined with rapid compensatory evolution can contribute  
262 to the recovery of symbiosis and local adaptation of hosts to changing environmental  
263 conditions. Partner-switching combined with rapid compensatory evolution could thus  
264 enhance the resilience of symbioses to environmental change, enabling the maintenance of  
265 their contribution to ecosystem function. Moreover, the potential fitness benefits of the  
266 phenotypic plasticity provided by partner-switching may select against the evolution of strict  
267 vertical transmission in symbioses that inhabit fluctuating or rapidly changing environments.

268

269

## 270 **Acknowledgements**

271 This work was funded by grants NE/K011774/2 and NE/V000128/1 from the Natural  
272 Environment Research Council, UK to M.A.B, D.D.C, and A.J.W and a White Rose DTP  
273 studentship from the Biotechnology and Biological Sciences Research Council, UK  
274 (BB/011151/1) to M.E.S.S. The funders had no role in the design of the study, the collection,  
275 analysis and interpretation of data or writing of the manuscript. We are grateful to Heather  
276 Walker for her technical assistance with the mass spectrometry.

277

278 **Author Contributions:** M.A.B, D.D.C, and M.E.S.S conceived and designed the study.  
279 M.E.S.S conducted experimental work. M.E.S.S and D.D.C analysed the data. M.E.S.S and  
280 M.A.B drafted the manuscript. All authors commented on the manuscript.

281

282 **Declaration of Interests:** The authors declare no competing interests.

283 **Figure Legends**

284

285 **Figure 1. Intergenomic epistasis of host symbiont growth rate and symbiont load**

286 **reaction norms.** For both A and B, each panel presents the data for a specific genotype of

287 *P. bursaria* host, as indicated at top of each panel, and the symbiont genotypes are

288 distinguished by colour. A) Initial growth rates of the host-symbiont pairings across a light

289 gradient over three days. The data points show the mean (n=3) initial growth rate  $\pm$ SE. The

290 host-symbiont growth rate reaction norm varied by symbiont genotype in the 186b host

291 genotype but did not vary in the HA1 or HK1 host genotypes, consistent with intergenomic

292 epistasis. B) Symbiont load of the host-symbiont pairings across a light gradient. The data

293 points show the mean (n=3) symbiont load, measured as relative chlorophyll fluorescence,

294  $\pm$ SE. The lines show polynomial models; the model coefficients showed a significant  $G^H \times G^S$

295 interaction (ANOVA,  $F_{8,36} = 27.22$  (the intercept); 8.58 (first coefficient); 6.09 (second

296 coefficient),  $P < 0.001$ ). For full statistical output see Data S1. The symbiont load reaction

297 norm varied by symbiont genotype in both the HK1 and 186b host genotypes but did not

298 vary in the HA1 host genotype, consistent with intergenomic epistasis. Related to Figure S2

299 and Table S1.

300

301 **Figure 2. Relative fitness reaction norms at the start and end of the evolution**

302 **experiment.** Panels show relative fitness reaction norms across a light gradient of various

303 host-symbiont pairings in the 186b host genotype in direct competition with the symbiont-

304 free 186b host genotype. The left-hand panel shows fitness reaction norms measured at the

305 start of the evolution experiment (T0) and the right-hand panel shows fitness reaction norms

306 measured at the end of the evolution experiment (T25), as indicated at the top of each

307 panel. Relative fitness was calculated as the selection rate, where a value above 0 indicates

308 a fitness benefit to the host of carrying algal symbionts. Colours show the symbiont

309 genotype treatment, where blue denotes that the 186b host carried the native 186b symbiont

310 genotype whereas grey denotes that the 186b host carried the non-native HK1 symbiont

311 genotype. Dark, thick lines show the mean (n=6) relative fitness reaction norms and light,

312 thin lines show the relative fitness reaction norms for each individual replicate. At the start of

313 the evolution experiment only the native host-symbiont pairing showed an increasing fitness

314 benefit of carrying symbionts with increasing irradiance, whereas at the end of the evolution

315 experiment both the native and non-native host symbiont pairings showed an increasing

316 fitness benefit of carrying symbionts with increasing irradiance. Related to Figure S3.

317

318

319 **Figure 3. Symbiont load reaction norms at the start and end of the evolution**  
320 **experiment.** Panels show symbiont load reaction norm across a light gradient of various  
321 host-symbiont pairings in the 186b host genotype. The left-hand panel shows symbiont load  
322 reaction norms measured at the start of the evolution experiment (T0) and the right-hand  
323 panel shows symbiont load reaction norms measured at the end of the evolution experiment  
324 (T25), as indicated at the top of each panel. Colours show the symbiont genotype treatment,  
325 where blue denotes that the 186b host carried the native 186b symbiont genotype whereas  
326 grey denotes that the 186b host carried the non-native HK1 symbiont genotype. Symbols  
327 show the mean ( $n=6$ )  $\pm$  standard error symbiont load and lines show the symbiont load  
328 reaction norms for each individual replicate. At the irradiance level used in the evolution  
329 experiment ( $50 \mu\text{E m}^{-2} \text{ s}^{-1}$ ), we observed that whereas mean symbiont load of the native  
330 symbiont had reduced, symbiont load of the non-native symbiont had increased, by the end  
331 of the evolution experiment. Related to Figure S3 and Table S3.

332

333

334 **Figure 4. Evolutionary trajectories of *Paramecium* and *Chlorella* metabolism.** Panels A  
335 and C show PCA plots for *P. bursaria* metabolism, while panels B and D show PCA plots for  
336 *Chlorella* metabolism, as indicated in the panel labels. The top row (A and B) plot PC1  
337 versus PC2. The bottom row (C and D) plot PC2 versus PC3. The percent variation  
338 explained by each PC is shown on the associated axis label. Colours show the symbiont  
339 genotype treatment, where blue denotes that the 186b host carried the native 186b symbiont  
340 genotype whereas grey denotes that the 186b host carried the non-native HK1 symbiont  
341 genotype. Dark points show ancestral metabolism at the state of the evolution experiment  
342 (mean of  $n=6$ ) whereas light points show the metabolism of each individual replicate  
343 population at the end of the evolution experiment (mean of  $n=3$  technical replicates per  
344 population). Arrows show the trajectory of metabolic evolution followed by each replicate  
345 population during the evolution experiment, and 95% confidence ellipses have been drawn  
346 for each treatment. The metabolite identifications for the top loadings are shown in their  
347 corresponding location. Related to Figure S4 and Table S2 & S3.

348

349

350 **STAR Methods**

351 **Resource availability**

352 **Lead contact**

353 Further information and requests for resources and reagents should be directed to and will  
354 be fulfilled by the Lead Contact, Michael Brockhurst  
355 (michael.brockhurst@manchester.ac.uk).

356

357 **Materials availability**

358 The natural strains used in this paper are available from culture collections (see below),  
359 unfortunately all our experimental populations were lost during the lab closures at the  
360 beginning of the global Covid pandemic.

361

362 **Data and code availability**

363 The data has been deposited within Mendeley Data (DOI: 10.17632/m7tpzttjx.1).

364

365 **Experimental Model and Subject Details**

366 The three natural strains of symbiotic *P. bursaria* used were: 186b (CCAP 1660/18) obtained  
367 from the Culture Collection for Algae and Protozoa (Oban, Scotland), and HA1 and HK1  
368 isolated in Japan and obtained from the Paramecium National Bio-Resource Project  
369 (Yamaguchi, Japan). *P. bursaria* stock cultures were maintained at 25°C under a 14:10 L:D  
370 cycle with 50  $\mu\text{E m}^{-2} \text{s}^{-1}$  of light (a high light condition). The stocks were maintained by batch  
371 culture in bacterized Protozoan Pellet Media (PPM, Carolina Biological Supply), made to a  
372 concentration of 0.66 g L<sup>-1</sup> with Volvic natural mineral water, and inoculated approximately  
373 20 hours prior to use with *Serratia marcescens* from frozen glycerol stocks.

374

375 To isolate *Chlorella* from the symbiosis, symbiotic cultures were first washed and  
376 concentrated with a 11  $\mu\text{m}$  nylon mesh using sterile Volvic. The suspension was then  
377 ultrasonicated using a Fisherbrand™ Q500 Sonicator (Fisher Scientific, NH, USA), at a  
378 power setting of 20% for 10 seconds sonification to disrupt the host cells. The liquid was  
379 then spotted onto Bold Basal Media plates (BBM)<sup>40</sup>, from which green colonies were

380 streaked out and isolated over several weeks. Plate stocks were maintained by streaking out  
381 one colony to a fresh plate every 3/4 weeks.

382

383 Symbiont-free *P. bursaria* were made by treating symbiotic cultures with paraquat (10 µg  
384 mL<sup>-1</sup>) for 3 to 7 days in high light conditions (>50 µE m<sup>-2</sup> s<sup>-1</sup>), until the host cells were visibly  
385 symbiont free. The cultures were then extensively washed with Volvic and closely monitored  
386 with microscopy and flow cytometry over a period of several weeks to check that re-greening  
387 by *Chlorella* did not occur. Stock cultures of the symbiont-free cells were maintained by  
388 batch culture at 25°C under a 14:10 L:D cycle with 3 µE m<sup>-2</sup> s<sup>-1</sup> of light and were given fresh  
389 PPM weekly. Symbiont-free *Paramecium* stocks have been maintained for a substantial  
390 period of time (months/years) without *Chlorella* ever being observed either inside or outside  
391 of *Paramecium* cells. In addition, using flow cytometry we have never observed chlorophyll  
392 fluorescence for *Paramecium* cells sampled from these stocks (methodology detailed in  
393 symbiont Load section). Together these tests confirm that paraquat treatment successfully  
394 removes all of the native *Chlorella*.

395

## 396 **Method Details**

### 397 *Cross infection*

398 Symbiont-free populations of the three *P. bursaria* strains were re-infected by adding a  
399 colony of *Chlorella* from the plate stocks derived from the appropriate strain. This was done  
400 with all three of the isolated *Chlorella* strains to construct all possible host-symbiont  
401 genotype pairings (n=9). The regreening process was followed by microscopy and took  
402 between 2-6 weeks. Over the process, cells were grown at the intermediate light level of 12  
403 µE m<sup>-2</sup> s<sup>-1</sup> and were given bacterized PPM weekly.

404

### 405 *Diagnostic PCR*

406 The correct algae genotype within the cross-infections was confirmed using diagnostic PCR.  
407 The *Chlorella* DNA was extracted by isolating the *Chlorella* and then using a standard 6%  
408 Chelex100 resin (Bio-Rad) extraction method. A nested PCR technique with overlapping,  
409 multiplex Chlorophyta specific primers were used as described by Hoshina et al. <sup>41</sup>.  
410 Standard PCR reactions were performed using Go Taq Green Master Mix (Promega) and  
411 0.5µmol L<sup>-1</sup> of the primer. The thermocycler programme was set to: 94°C for 5min, 30 cycles  
412 of (94°C for 30sec, 55°C for 30sec, 72°C for 60sec), and 5 min at 72°C.

413

414

415



416 *Growth rate*

417 Growth rates of the host-symbiont pairings were measured across a light gradient. The cells  
418 were washed and concentrated with a 11µm nylon mesh using sterile Volvic and re-  
419 suspended in bacterized PPM. The cultures were then split and acclimated to their treatment  
420 light condition (0, 12, 24, & 50 µE m<sup>-2</sup> s<sup>-1</sup>) for five days. The cultures were then re-suspended  
421 in bacterized PPM to a target cell density of 150 cell mL<sup>-1</sup>. Cell densities were measured at  
422 0, 24, 48 and 72 hours by fixing 360µL of each cell culture, in triplicate, in 1% v/v  
423 glutaraldehyde in 96-well flat-bottomed micro-well plates. Images were taken with a plate  
424 reader (Tecan Spark 10M) and cell counts were made using an automated image analysis  
425 macro in ImageJ v1.50i<sup>42</sup>. The initial host-symbiont growth rate was measured over a period  
426 of three days.

427

428 *Symbiont load*

429 The symbiont load (i.e., the number of symbionts per host cell) was measured in cultures  
430 derived from the growth rate experiment so that the data could be integrated between the  
431 two measurements. Triplicate 300µl samples of each cell culture were taken from 72-hour  
432 cultures for flow cytometry analysis. Host symbiont load was estimated using a CytoFLEX S  
433 flow cytometer (Beckman Coulter Inc., CA, USA) by measuring the intensity of chlorophyll  
434 fluorescence for single *P. bursaria* cells (excitation 488nm, emission 690/50nm) and gating  
435 cell size using forward side scatter; a method established by Kadono et al.<sup>19</sup>. The  
436 measurements were calibrated against 8-peak rainbow calibration particles (BioLegend),  
437 and then presented as relative fluorescence to reduce variation across sampling sessions.

438

439 *Partner switching*

440 Metabolomics experiment

441 Cultures of the host-symbiont pairings were washed and concentrated with a 11µm nylon  
442 mesh using sterile Volvic and re-suspended in bacterized PPM. The cultures were then split  
443 and acclimated at their treatment light condition (0, 12 & 50 µE m<sup>-2</sup> s<sup>-1</sup>) for seven days. The  
444 symbiotic partners were separated in order to get *P. bursaria* and *Chlorella* metabolic  
445 fraction. The *P. bursaria* cells were concentrated with a 11µm nylon mesh using Volvic and  
446 then the *P. bursaria* cells were disrupted by sonication (20% power for 10 secs). 1ml of the  
447 lysate was pushed through a 1.6µm filter, which caught the intact *Chlorella* cells, and the  
448 run-through was collected and stored as the *P. bursaria* fraction. The 1.6µm filter was  
449 washed with 5ml cold deionized water, and then reversed so that the *Chlorella* cells were  
450 resuspended in 1ml of cold methanol, which was stored as the *Chlorella* fraction. After which  
451 the *Chlorella* fraction samples were already in methanol, but the *P. bursaria* fraction samples  
452 had then to be diluted by 50% with methanol.

453 Mass spectrometry

454 Metabolic profiles were recorded using ESI ToF-MS, on the Qstar Elite with automatic  
455 injection using Waters Alliance 2695 HPLC (no column used), in positive mode. This is an  
456 established high-throughput method with a large mass range (50 Da to 1000 Da).

457

458 The mass spectrometry settings were: positive polarity, 4.2kV Ion Spray voltage, 120V  
459 Declustering potential, 265V Focusing potential, 200°C Source temperature, 40 ml min<sup>-1</sup> Gas  
460 Flow, the solvent was 50:50 methanol to water at flow rate 40µl min<sup>-1</sup> and the injected  
461 volume was 10µl.

462

463 The processing was performed using in-house software Visual Basic macro 216<sup>43</sup>, which  
464 combined the spectra across the technical replicates by binning the crude m/z values into  
465 0.2-unit bins. The relative mass abundances (% total ion count) for each bin was summed.  
466 Pareto scaling was applied to the results, and the data was then analysed by principal  
467 component analysis using SIMCA-P software (Umetrics). When treatment-based separation  
468 was observed, supervised orthogonal partial least squares discriminant analysis (OPLS-DA)  
469 separation was then performed using the discriminatory treatment with the SIMCA-P  
470 software.

471

472 Identification of significant masses

473 Masses of interest were annotated using the initial identifications from the in-house  
474 software program and further comparisons against KEGG (<https://www.genome.jp/kegg/>)  
475<sup>44,45</sup> and Metlin (<https://metlin.scripps.edu>)<sup>46</sup> databases. The Metabolomics Standards  
476 Initiative requires two independent measures to confirm identity, this partner-switching  
477 metabolomic analysis only used one measure (accurate mass) and therefore, meets only the  
478 level 2 requirements of putative annotated compounds.

479

480 *Evolution Experiment*

481 The populations used derive from the cross-infections and, therefore, the  
482 host-symbiont pairings come from the same cured 186b ancestor that was then re-infected  
483 with either its native (186b) or non-native (HK1) symbionts. The two host-symbiont pairings  
484 were split into six replicate populations that were used as the starting populations. The  
485 200ml populations were propagated by weekly serial transfer for 25 transfers at a high light  
486 (50 µE m<sup>-2</sup> s<sup>-1</sup>) 14:10 L:D cycle. At every transfer, cell-density was equalised to 100 cells mL<sup>-1</sup>  
487 and the transferred cells were washed with a 11µm nylon mesh using Volvic before being  
488 re-suspended in bacterized PPM. Cell density was measured before and after each transfer  
489 by fixing 360µL of each cell culture, in triplicate, in 1% v/v glutaraldehyde in 96-well flat-

490 bottomed micro-well plates. Images were taken with a plate reader (Tecan Spark 10M) and  
491 cell counts were made using an automated image analysis macro in ImageJ v1.50i<sup>42</sup>.  
492 Growth rate and symbiont load assays were conducted at the start, T10, T20 and end of the  
493 experiment using the method described above.

494

#### 495 Fitness assay

496 Fitness assays were conducted at the start and end of the evolution experiment. *P. bursaria*  
497 cultures, both the symbiotic pairings and the symbiont-free ancestor, were washed with  
498 Volvic and resuspended in bacterized PPM. The cultures were then split and acclimated at  
499 their treatment light level (0,12,50  $\mu\text{E m}^{-2} \text{s}^{-1}$ ) for five days. Cell densities were counted by  
500 fixing 360 $\mu\text{L}$  of each cell culture, in triplicate, in 1% v/v glutaraldehyde in 96-well flat-  
501 bottomed micro-well plates. Images were taken with a plate reader (Tecan Spark 10M) and  
502 cell counts were made using an automated image analysis macro in ImageJ v1.50i<sup>42</sup>. The  
503 competitions were started by setting up microcosms that each contained 50:50 populations  
504 of green and white cells (with target values of 20 green cells and 20 white cells per mL) that  
505 were in direct competition. Cells were sampled on day 0 and day 7 on a flow cytometer and  
506 the proportion of green to white cells was measured and used to calculate the selection rate.  
507 Selection rate (R) is calculated as the difference in Malthusian parameters of green (test)  
508 versus white (reference) cell populations in direct competition:  $R = (\ln(\text{test}_{\text{start}}/\text{test}_{\text{end}}) -$   
509  $\ln(\text{reference}_{\text{start}}/\text{reference}_{\text{end}})) / \text{day}$ <sup>47</sup>. Green versus white cells were distinguished using  
510 single cell fluorescence estimated using a CytoFLEX S flow cytometer (Beckman Coulter  
511 Inc., CA, USA) by measuring the intensity of chlorophyll Fluorescence (excitation 488nm,  
512 emission 690/50nm) and gating cell size using forward side scatter; a method established by  
513 Kadono et al.<sup>19</sup>. The measurements were calibrated against 8-peak rainbow calibration  
514 particles (BioLegend), and then presented as relative fluorescence to reduce variation  
515 across sampling sessions. The re-establishment of endosymbiosis takes between 2-4  
516 weeks, and this method was tested to ensure that the symbiont-free cells do not re-green  
517 over the course of the experiment.

518

#### 519 Metabolomics

520 The cultures were sampled at the start and end of the evolution experiment. Cultures were  
521 washed and concentrated with a 11 $\mu\text{m}$  nylon mesh using Volvic and re-suspended in  
522 bacterized PPM. The cultures were acclimated at their treatment light condition (50  $\mu\text{E m}^{-2} \text{s}^{-1}$ )  
523 for seven days. At the start of the evolution experiment we analysed a sample from each  
524 of the 6 replicate populations per treatment to determine the ancestral metabolomes of each  
525 host-symbiont pairing (i.e., n=6). At the end of the evolution experiment, we increased our  
526 replication such that for each of the 6 replicate populations per treatment we analysed 3

527 technical replicates, allowing us to determine differences between replicate populations as  
528 well as between treatments in their evolved metabolomes. At each sampling event, the  
529 symbiotic partners were separated in order to get *P. bursaria* and *Chlorella* metabolic  
530 fraction using the extraction method described above. Samples were freeze-dried for  
531 storage, and then resuspended in 50:50 methanol to water prior to mass spectrometry.

532

533 The samples were analysed with a Synapt G2-Si with Acuity UPLC, recording in positive  
534 mode over a large untargeted mass range (50 – 1000 Da). A 2.1x50mm Acuity UPLC BEH  
535 C18 column was used with acetonitrile as the solvent. The machine settings are listed in  
536 detail below:

537

538 The mass spectrometry settings were: positive polarity, 2.3kV Capillary voltage, 20V Sample  
539 Cone voltage, 100°C Source Temperature, 280°C Desolvation temperature, 600 L hr<sup>-1</sup> Gas  
540 Flow, 5µl Injected volume and 45°C Column temperature. The gradient started at time 0 with  
541 95% water to 5% acetonitrile, at 3 minutes it was 65% water to 35% acetonitrile, at 6  
542 minutes it was 0% water to 100% acetonitrile, at 7.5 minutes it was 0% water to 100%  
543 acetonitrile, and at 7.6 minutes it was 95% water to 5% acetonitrile.

544

545 The *P. bursaria* and *Chlorella* fraction were analysed separately. The xcms R package<sup>48-50</sup>  
546 was used to extract the spectra from the CDF data files, using a step argument of 0.01 m/z.  
547 Peaks were identified, and then grouped across samples. These aligned peaks were used to  
548 identify and correct correlated drifts in retention time from run to run. Pareto scaling was  
549 applied to the resulting intensity matrix.

550

551 Metabolomics analysis

552 The metabolic profiles from the start and end of the experiment were compared using  
553 principal component analysis (PCA) with the prcomp() function in Base R  
554 (<https://www.rproject.org/>). For both fractions the first three components were considered,  
555 this accounted for >88% of the variance. The top 1% of the loadings were selected using the  
556 absolute magnitude of the loadings. These top loadings were identified where possible, and  
557 the identified loadings were then depicted in their associated component space. The relative  
558 abundance of these top loadings was visualised using heatmaps drawn with the heatmap.2()  
559 function from the gplot package<sup>51</sup>. The phylogenies were based on UPGMA clustering of the  
560 PCA coordinates of the samples using the hclust() function. This approach of integrating  
561 metabolic data and genotypes in heatmaps has been used previously<sup>52</sup>.

562

563 Identification of significant masses

564 Masses of interest were investigated using the MarVis-Suite 2.0 software  
565 (<http://marvis.gobics.de/>)<sup>53</sup>, using retention time and mass to compare against KEGG  
566 (<https://www.genome.jp/kegg/>)<sup>44,45</sup> and MetaCyc (<https://biocyc.org/>)<sup>54</sup> databases. The  
567 Metabolomics Standards Initiative requires two independent measures to confirm identity,  
568 which the combination of retention time and accurate mass achieves for the analysis of the  
569 evolution experiment metabolomics.

570

## 571 **Quantification and Statistical analysis**

572 Statistical analyses were performed in Rv.3.5.0<sup>55</sup> and all plots were produced using  
573 package ggplot2<sup>56</sup> unless otherwise stated. Physiology tests were analysed by both ANOVA  
574 and ANCOVA, with transfer time, host and symbiont identity as factors. A linear mixed effect  
575 model was used to analysis the growth rate per transfer using lm() function from the nlme  
576 package<sup>57</sup>. The lm model included fixed effects of symbiont genotype and transfer number,  
577 and random effects of transfer number given sample ID. Where parametric tests were used  
578 the data conformed to parametric assumptions of independence, normality and homogeneity  
579 of variance, which was confirmed using the appropriate tests and plots (e.g normal QQ and  
580 residual vs fitted values). Summary details of the data is provided in the figure legends (e.g  
581 the value of n and type of error used) and details of the statistical methods used are within  
582 the supplementary statistics data (Data S1).

583

584 Within all of our experiments the spatial arrangement of cultures in the incubator was fully  
585 randomised to ensure statistical independence. For the short term assays the spatial  
586 randomisation was reassigned every day. For the long-term evolution experiment the spatial  
587 randomisation was reassigned at each weekly serial transfer.

588

## 589 **Supplementary data file legend**

590 **Data S1. Statistical outputs and model parameters for analyses associated with the**  
591 **figures of the main manuscript and supplementary figures. Related to Figures 1-3 &**  
592 **S3 and STAR Methods.**

593 A.) Data S1A is related to Figure 1: the first section presents an ANOVA and Welch two  
594 sample t-test related to Figure 1A, the second section presents an ANOVA and polynomial  
595 model related to Figure 1B. B.) Data S1B presents an ANOVA model related to Figure 2. C)  
596 Data S1C presents an ANOVA model related to Figure 3. D) Data S1D is related to Figure  
597 S3: the first section presents a linear mixed effect model related to Figure S3A, the second

598 section presents a Welch two sample t-test related to Figure S3B. In all relevant statistical  
599 models, light is treated as a continuous variable.

600

601

602

603

604 **References:**

- 605 1. Sachs, J.L., and Simms, E.L. (2006). Pathways to mutualism breakdown. *Trends in*  
606 *Ecology & Evolution* 21, 585–592.
- 607 2. Boulotte, N.M., Dalton, S.J., Carroll, A.G., Harrison, P.L., Putnam, H.M., Peplow, L.M.,  
608 and van Oppen, M.J. (2016). Exploring the *Symbiodinium* rare biosphere provides  
609 evidence for symbiont switching in reef-building corals. *The ISME Journal* 10, 2693–  
610 2701.
- 611 3. Lefèvre, C., Charles, H., Vallier, A., Delobel, B., Farrell, B., and Heddi, A. (2004).  
612 Endosymbiont Phylogenesis in the Dryophthoridae Weevils: Evidence for Bacterial  
613 Replacement. *Mol Biol Evol* 21, 965–973.
- 614 4. Koga, R., and Moran, N.A. (2014). Swapping symbionts in spittlebugs: evolutionary  
615 replacement of a reduced genome symbiont. *The ISME Journal* 8, 1237–1246.
- 616 5. Matsuura, Y., Moriyama, M., Łukasik, P., Vanderpool, D., Tanahashi, M., Meng, X.-Y.,  
617 McCutcheon, J.P., and Fukatsu, T. (2018). Recurrent symbiont recruitment from fungal  
618 parasites in cicadas. *PNAS* 115, E5970–E5979.
- 619 6. Heath, K.D. (2010). Intergenomic Epistasis and Coevolutionary Constraint in Plants and  
620 Rhizobia. *Evolution* 64, 1446–1458.
- 621 7. Thompson, J.N. (2005). *The Geographic Mosaic of Coevolution* (University of Chicago  
622 Press).
- 623 8. Heath, K.D., and Tiffin, P. (2007). Context dependence in the coevolution of plant and  
624 rhizobial mutualists. *Proceedings of the Royal Society of London B: Biological Sciences*  
625 274, 1905–1912.
- 626 9. Joy, J.B. (2013). Symbiosis catalyses niche expansion and diversification. *Proceedings*  
627 *of the Royal Society B: Biological Sciences* 280, 20122820.
- 628 10. Sudakaran, S., Kost, C., and Kaltenpoth, M. (2017). Symbiont Acquisition and  
629 Replacement as a Source of Ecological Innovation. *Trends in Microbiology* 25, 375–390.
- 630 11. Jaenike, J., Unckless, R., Cockburn, S.N., Boelio, L.M., and Perlman, S.J. (2010).  
631 Adaptation via Symbiosis: Recent Spread of a *Drosophila* Defensive Symbiont. *Science*  
632 329, 212–215.
- 633 12. Jiggins, F.M., and Hurst, G.D.D. (2011). Rapid Insect Evolution by Symbiont Transfer.  
634 *Science* 332, 185–186.

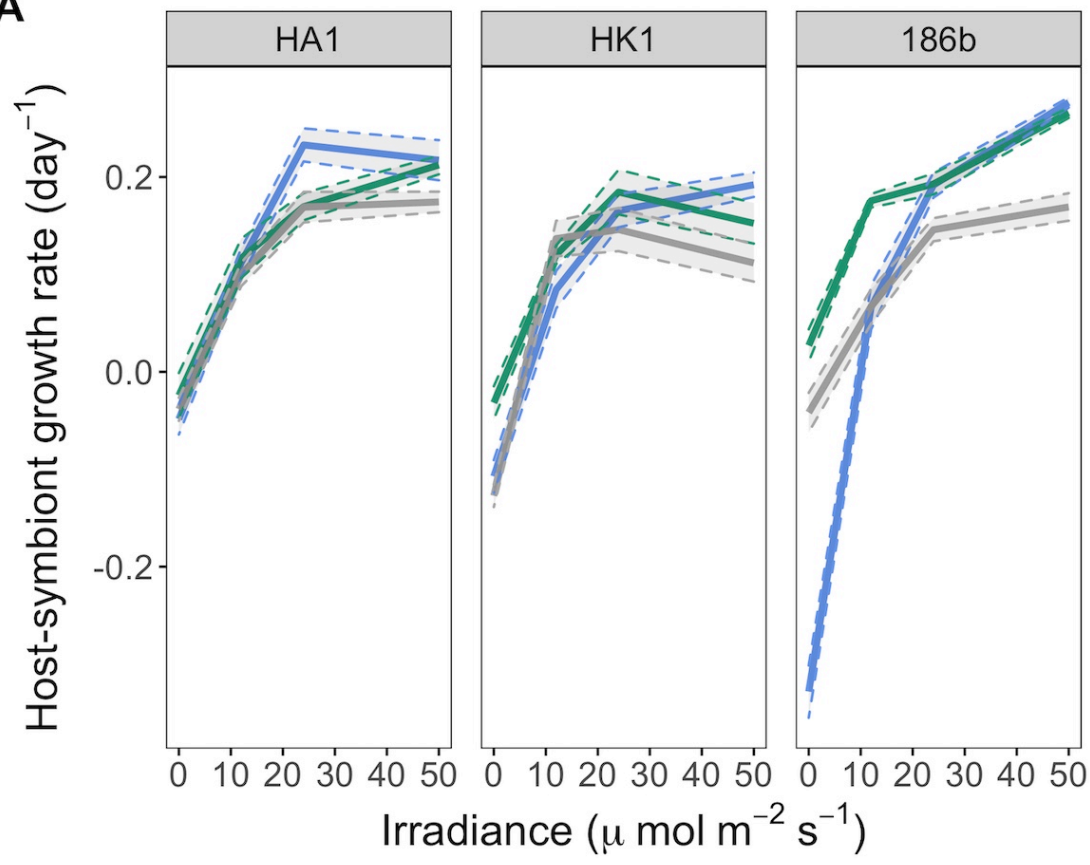
- 635 13. Matthews, J.L., Oakley, C.A., Lutz, A., Hillyer, K.E., Roessner, U., Grossman, A.R.,  
636 Weis, V.M., and Davy, S.K. (2018). Partner switching and metabolic flux in a model  
637 cnidarian–dinoflagellate symbiosis. *Proceedings of the Royal Society B: Biological*  
638 *Sciences* 285, 20182336.
- 639 14. Russell, J.A., and Moran, N.A. (2005). Horizontal Transfer of Bacterial Symbionts:  
640 Heritability and Fitness Effects in a Novel Aphid Host. *Appl. Environ. Microbiol.* 71,  
641 7987–7994.
- 642 15. McGraw, E.A., Merritt, D.J., Droller, J.N., and O’Neill, S.L. (2002). *Wolbachia* density  
643 and virulence attenuation after transfer into a novel host. *PNAS* 99, 2918–2923.
- 644 16. Nakayama, S., Parratt, S.R., Hutchence, K.J., Lewis, Z., Price, T. a. R., and Hurst,  
645 G.D.D. (2015). Can maternally inherited endosymbionts adapt to a novel host? Direct  
646 costs of *Spiroplasma* infection, but not vertical transmission efficiency, evolve rapidly  
647 after horizontal transfer into *D. melanogaster*. *Heredity* 114, 539–543.
- 648 17. Sullivan, J.T., Patrick, H.N., Lowther, W.L., Scott, D.B., and Ronson, C.W. (1995).  
649 Nodulating strains of *Rhizobium loti* arise through chromosomal symbiotic gene transfer  
650 in the environment. *PNAS* 92, 8985–8989.
- 651 18. Johnson, M.D. (2011). The acquisition of phototrophy: adaptive strategies of hosting  
652 endosymbionts and organelles. *Photosynth Res* 107, 117–132.
- 653 19. Kadono, T., Kawano, T., Hosoya, H., and Kosaka, T. (2004). Flow cytometric studies of  
654 the host-regulated cell cycle in algae symbiotic with green paramecium. *Protoplasma*  
655 223, 133–141.
- 656 20. Ziesenisz, E., Reisser, W., and Wiessner, W. (1981). Evidence of de novo synthesis of  
657 maltose excreted by the endosymbiotic *Chlorella* from *Paramecium bursaria*. *Planta* 153,  
658 481–485.
- 659 21. Kodama, Y., and Fujishima, M. (2011). Four important cytological events needed to  
660 establish endosymbiosis of symbiotic *Chlorella* sp. to the alga-free *Paramecium*  
661 *bursaria*. *Japanese Journal of Protozoology* 44, 1–20.
- 662 22. Siegel, R.W. (1960). Hereditary endosymbiosis in *Paramecium bursaria*. *Experimental*  
663 *Cell Research* 19, 239–252.
- 664 23. Sørensen, M.E., Wood, A.J., Minter, E.J., Lowe, C.D., Cameron, D.D., and Brockhurst,  
665 M.A. (2020). Comparison of independent evolutionary origins reveals both convergence  
666 and divergence in the metabolic mechanisms of symbiosis. *Current Biology*.
- 667 24. Lowe, C.D., Minter, E.J., Cameron, D.D., and Brockhurst, M.A. (2016). Shining a Light  
668 on Exploitative Host Control in a Photosynthetic Endosymbiosis. *Current Biology* 26,  
669 207–211.
- 670 25. Dean, A.D., Minter, E.J.A., Sørensen, M.E.S., Lowe, C.D., Cameron, D.D., Brockhurst,  
671 M.A., and Jamie Wood, A. (2016). Host control and nutrient trading in a photosynthetic  
672 symbiosis. *Journal of Theoretical Biology* 405, 82–93.
- 673 26. Minter, E.J.A., Lowe, C.D., Sørensen, M.E.S., Wood, A.J., Cameron, D.D., and  
674 Brockhurst, M.A. (2018). Variation and asymmetry in host-symbiont dependence in a  
675 microbial symbiosis. *BMC Evol Biol* 18, 108.

- 676 27. Mallick, N. (2004). Copper-induced oxidative stress in the chlorophycean microalga  
677 *Chlorella vulgaris*: response of the antioxidant system. *J. Plant Physiol.* *161*, 591–597.
- 678 28. Shiu, C.-T., and Lee, T.-M. (2005). Ultraviolet-B-induced oxidative stress and responses  
679 of the ascorbate-glutathione cycle in a marine macroalga *Ulva fasciata*. *J. Exp. Bot.* *56*,  
680 2851–2865.
- 681 29. Kodama, Y., and Fujishima, M. (2008). Cycloheximide Induces Synchronous Swelling of  
682 Perialgal Vacuoles Enclosing Symbiotic *Chlorella vulgaris* and Digestion of the Algae in  
683 the Ciliate *Paramecium bursaria*. *Protist* *159*, 483–494.
- 684 30. Kodama, Y., and Fujishima, M. (2012). Cell division and density of symbiotic *Chlorella*  
685 *variabilis* of the ciliate *Paramecium bursaria* is controlled by the host's nutritional  
686 conditions during early infection process. *Environmental Microbiology* *14*, 2800–2811.
- 687 31. Cantin, N.E., van Oppen, M.J.H., Willis, B.L., Mieog, J.C., and Negri, A.P. (2009).  
688 Juvenile corals can acquire more carbon from high-performance algal symbionts. *Coral*  
689 *Reefs* *28*, 405.
- 690 32. Freeman, C.J., Thacker, R.W., Baker, D.M., and Fogel, M.L. (2013). Quality or quantity:  
691 is nutrient transfer driven more by symbiont identity and productivity than by symbiont  
692 abundance? *The ISME Journal* *7*, 1116–1125.
- 693 33. Husnik, F., and McCutcheon, J.P. (2016). Repeated replacement of an intrabacterial  
694 symbiont in the tripartite nested mealybug symbiosis. *PNAS* *113*, E5416–E5424.
- 695 34. Rolshausen, G., Grande, F.D., Sadowska-Deś, A.D., Otte, J., and Schmitt, I. (2018).  
696 Quantifying the climatic niche of symbiont partners in a lichen symbiosis indicates  
697 mutualist-mediated niche expansions. *Ecography* *41*, 1380–1392.
- 698 35. Matthews, J.L., Oakley, C.A., Lutz, A., Hillyer, K.E., Roessner, U., Grossman, A.R.,  
699 Weis, V.M., and Davy, S.K. (2018). Partner switching and metabolic flux in a model  
700 cnidarian–dinoflagellate symbiosis. *Proceedings of the Royal Society B: Biological*  
701 *Sciences* *285*, 20182336.
- 702 36. Weis, V.M. (2008). Cellular mechanisms of Cnidarian bleaching: stress causes the  
703 collapse of symbiosis. *Journal of Experimental Biology* *211*, 3059–3066.
- 704 37. Abrego, D., Ulstrup, K.E., Willis, B.L., and van Oppen, M.J.H. (2008). Species-specific  
705 interactions between algal endosymbionts and coral hosts define their bleaching  
706 response to heat and light stress. *Proceedings of the Royal Society B: Biological*  
707 *Sciences* *275*, 2273–2282.
- 708 38. Ye, S., Bhattacharjee, M., and Siemann, E. (2019). Thermal Tolerance in Green Hydra:  
709 Identifying the Roles of Algal Endosymbionts and Hosts in a Freshwater Holobiont Under  
710 Stress. *Microb Ecol* *77*, 537–545.
- 711 39. Howells, E.J., Beltran, V.H., Larsen, N.W., Bay, L.K., Willis, B.L., and van Oppen, M.J.H.  
712 (2012). Coral thermal tolerance shaped by local adaptation of photosymbionts. *Nature*  
713 *Climate Change* *2*, 116–120.
- 714 40. Stein, J.R. (1979). (ED.) *Handbook of Phycological Methods: Culture Methods and*  
715 *Growth Measurements* (Cambridge University Press).



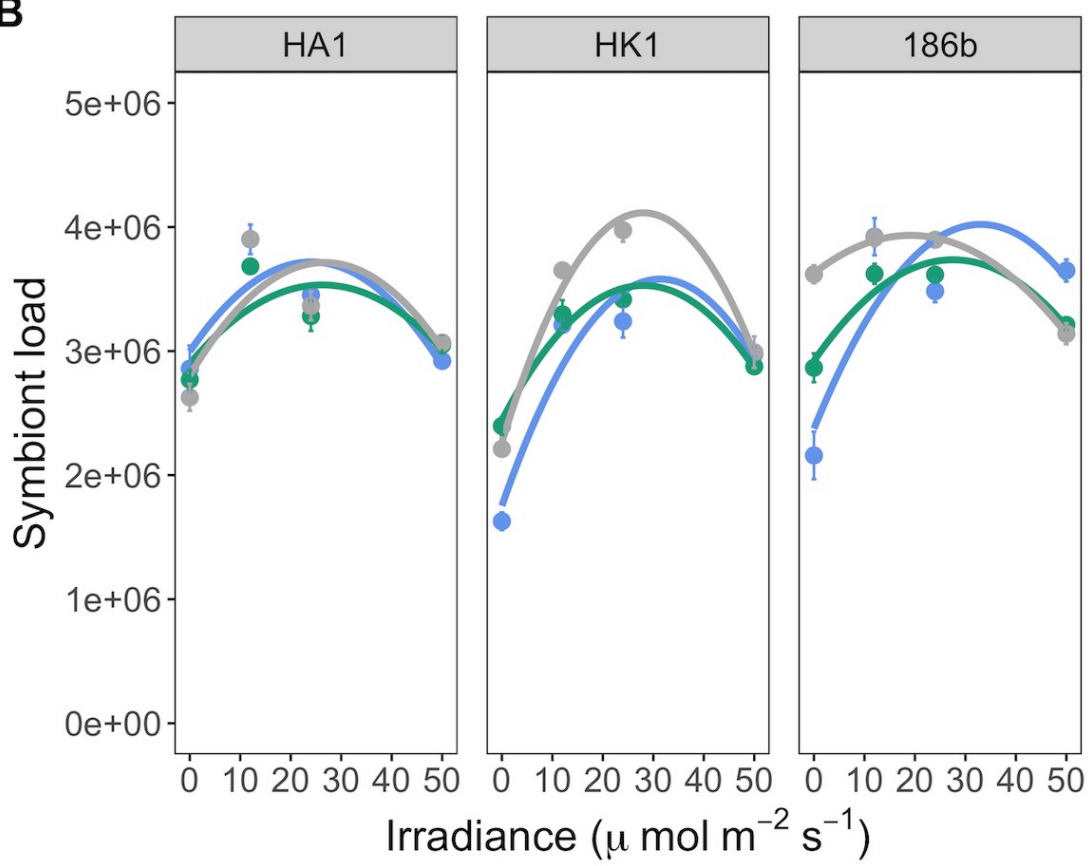
- 716 41. Hoshina, R., Kato, Y., Kamako, S., and Imamura, N. (2005). Genetic Evidence of  
717 “American” and “European” Type Symbiotic Algae of *Paramecium bursaria* Ehrenberg.  
718 *Plant Biol (Stuttg)* 7, 526–532.
- 719 42. Schneider, C.A., Rasband, W.S., and Eliceiri, K.W. (2012). NIH Image to ImageJ: 25  
720 years of image analysis. *Nature Methods*. <https://www.nature.com/articles/nmeth.2089>.
- 721 43. Overy, S.A., Walker, H.J., Malone, S., Howard, T.P., Baxter, C.J., Sweetlove, L.J., Hill,  
722 S.A., and Quick, W.P. (2005). Application of metabolite profiling to the identification of  
723 traits in a population of tomato introgression lines. *J Exp Bot* 56, 287–296.
- 724 44. Kanehisa, M., and Goto, S. (2000). KEGG: kyoto encyclopedia of genes and genomes.  
725 *Nucleic Acids Res.* 28, 27–30.
- 726 45. Kanehisa, M., Sato, Y., Furumichi, M., Morishima, K., and Tanabe, M. (2019). New  
727 approach for understanding genome variations in KEGG. *Nucleic Acids Res.* 47, D590–  
728 D595.
- 729 46. Smith, C.A., O’Maille, G., Want, E.J., Qin, C., Trauger, S.A., Brandon, T.R., Custodio,  
730 D.E., Abagyan, R., and Siuzdak, G. (2005). METLIN: a metabolite mass spectral  
731 database. *Ther Drug Monit* 27, 747–751.
- 732 47. Lenski, R.E., Rose, M.R., Simpson, S.C., and Tadler, S.C. (1991). Long-Term  
733 Experimental Evolution in *Escherichia coli*. I. Adaptation and Divergence During 2,000  
734 Generations. *The American Naturalist* 138, 1315–1341.
- 735 48. Benton, H.P., Want, E.J., and Ebbels, T.M.D. (2010). Correction of mass calibration  
736 gaps in liquid chromatography-mass spectrometry metabolomics data. *Bioinformatics*  
737 26, 2488–2489.
- 738 49. Smith, C.A., Want, E.J., O’Maille, G., Abagyan, R., and Siuzdak, G. (2006). XCMS:  
739 Processing Mass Spectrometry Data for Metabolite Profiling Using Nonlinear Peak  
740 Alignment, Matching, and Identification. *Anal. Chem.* 78, 779–787.
- 741 50. Tautenhahn, R., Böttcher, C., and Neumann, S. (2008). Highly sensitive feature  
742 detection for high resolution LC/MS. *BMC Bioinformatics* 9, 504.
- 743 51. Warnes, G.R., Bolker, B., Bonebakker, L., Gentleman, R., Huber, W., Liaw, A., Lumley,  
744 T., Maechler, M., Magnusson, A., and Moeller, S. (2009). gplots: Various R programming  
745 tools for plotting data. R package version 2, 1.
- 746 52. Cotton, T.E.A., Pétriacq, P., Cameron, D.D., Meselmani, M.A., Schwarzenbacher, R.,  
747 Rolfe, S.A., and Ton, J. (2019). Metabolic regulation of the maize rhizobiome by  
748 benzoxazinoids. *ISME J* 13, 1647–1658.
- 749 53. Kaefer, A., Lingner, T., Feussner, K., Göbel, C., Feussner, I., and Meinicke, P. (2009).  
750 MarVis: a tool for clustering and visualization of metabolic biomarkers. *BMC*  
751 *Bioinformatics* 10, 92.
- 752 54. Caspi, R., Billington, R., Fulcher, C.A., Keseler, I.M., Kothari, A., Krummenacker, M.,  
753 Latendresse, M., Midford, P.E., Ong, Q., Ong, W.K., et al. (2018). The MetaCyc  
754 database of metabolic pathways and enzymes. *Nucleic Acids Res* 46, D633–D639.
- 755 55. R Core Team (2018). R: A Language and Environment for Statistical Computing.

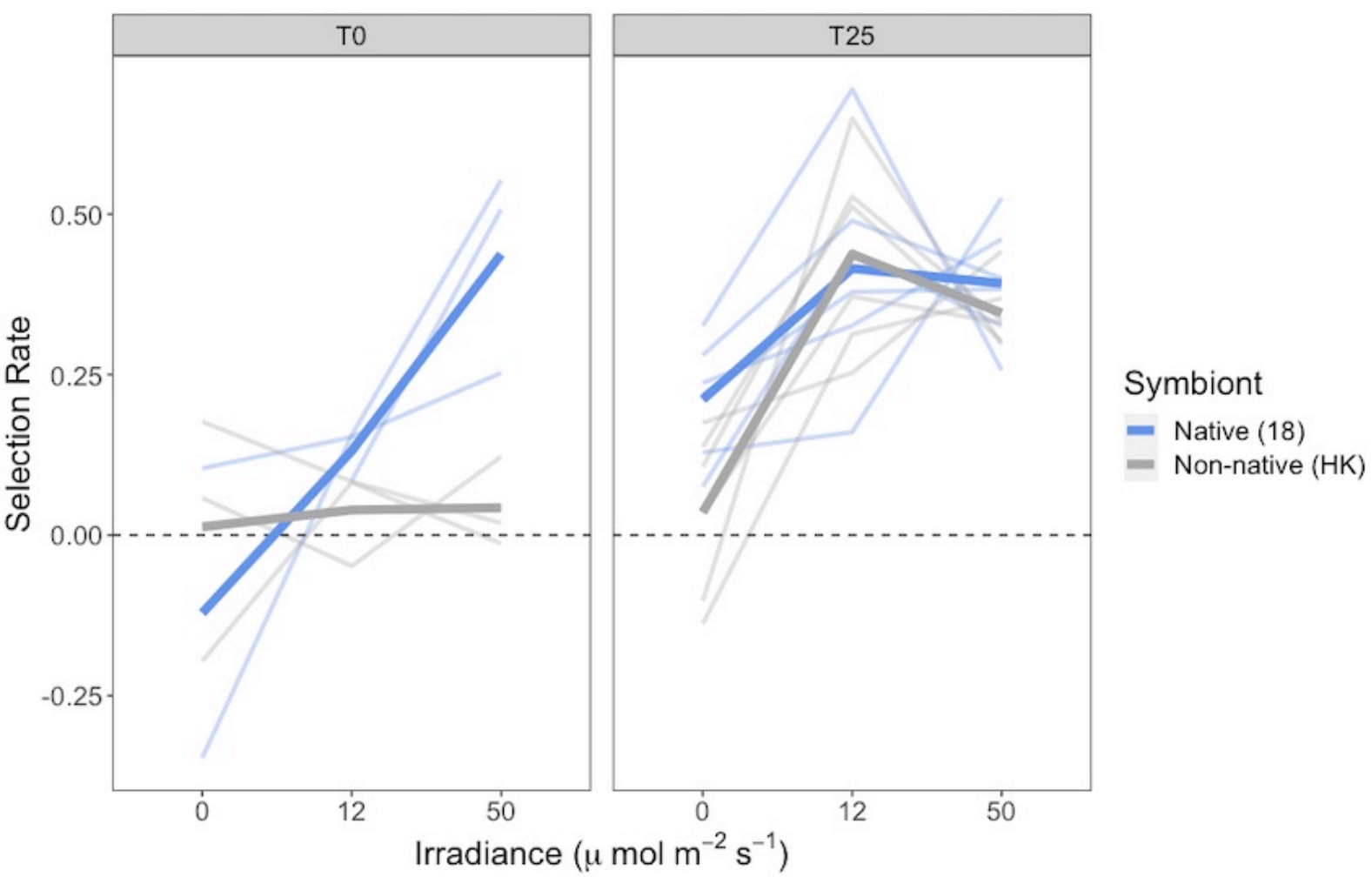
- 756 56. Wickham, H. (2016). ggplot2: Elegant Graphics for Data Analysis.
- 757 57. Pinheiro, J., Bates, D., DebRoy, S., Sarkar, D., and R core Team (2019) (2019). nlme:  
758 Linear and Nonlinear Mixed Effects Models.
- 759

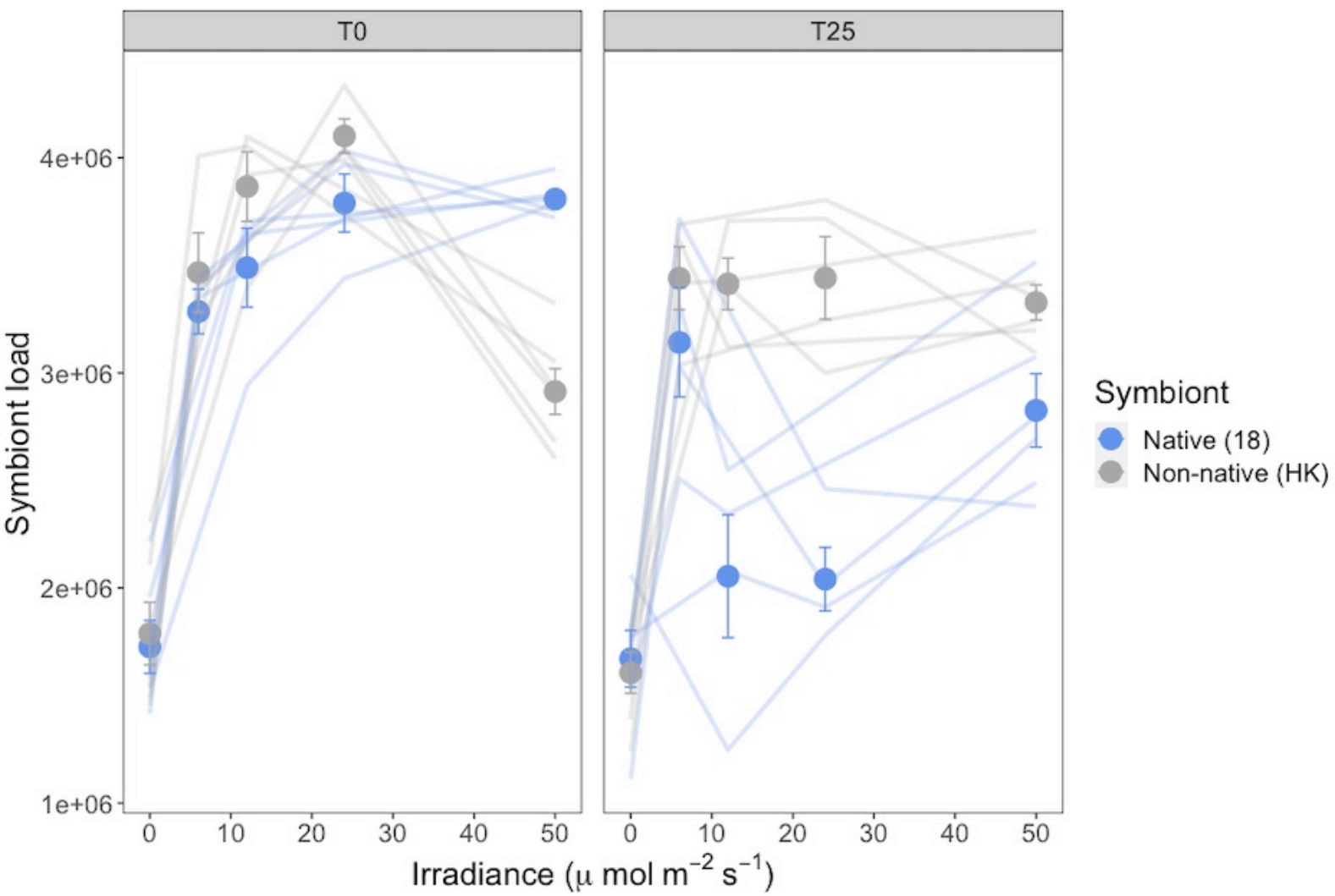
**A**

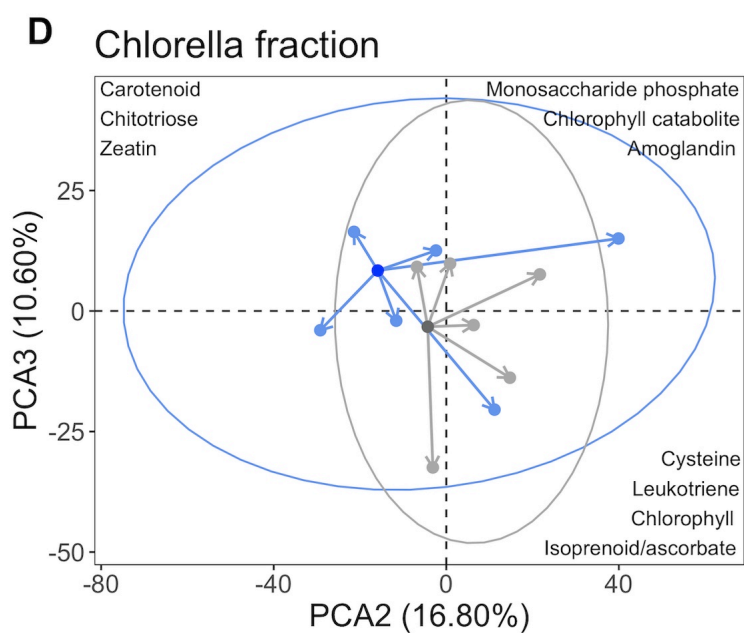
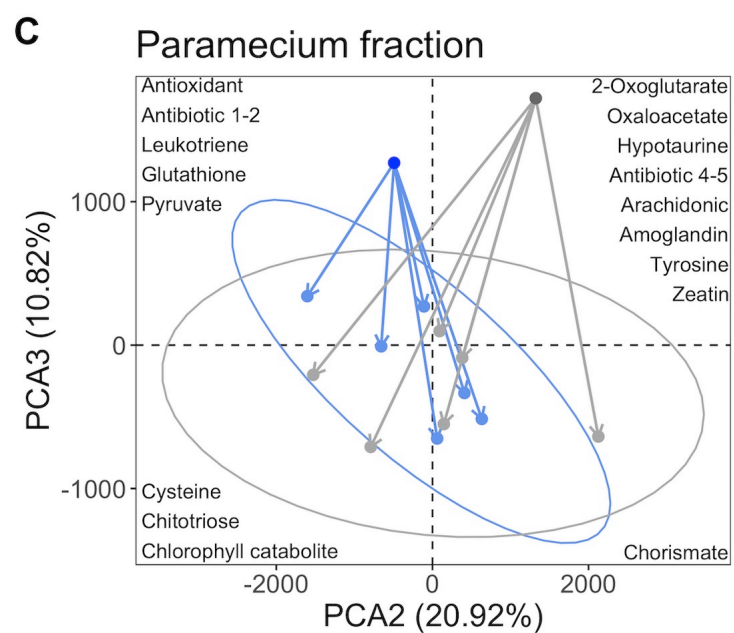
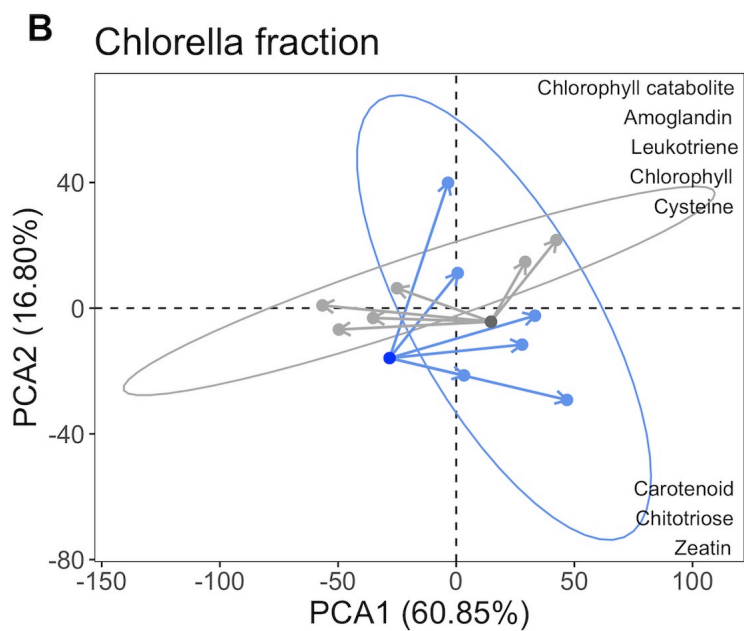
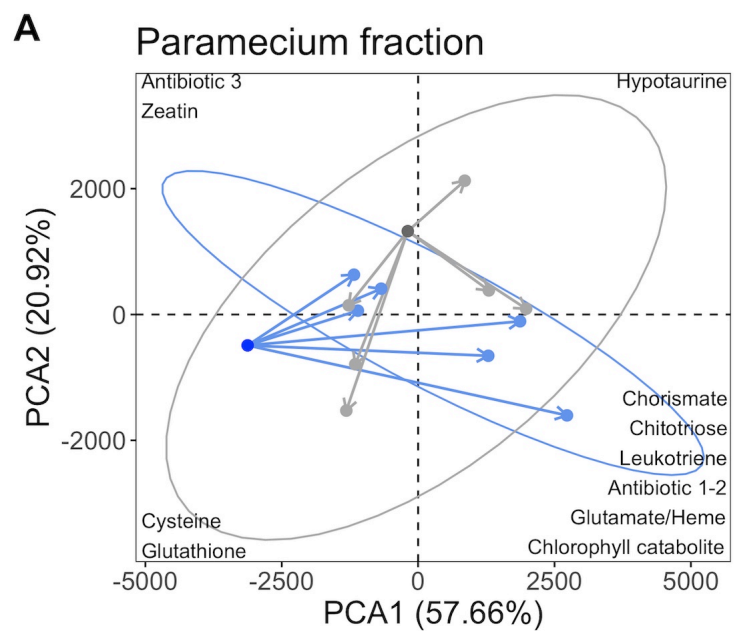
Symbiont genotype

- 18
- HA
- HK

**B**







Group ◆ 18 ◆ 18start ◆ HK ◆ HKstart